Electrostatic Plasma Membrane Targeting is Essential for Dlg Function in Cell Polarity and Tumorigenesis

Juan Lu[1*], Wei Dong[1*], Yan Tao[2], and Yang Hong[1]

1. Department of Cell Biology, University of Pittsburgh Medical School, Pittsburgh, PA 15261, USA

2. Jiangsu University, Zhengjiang, Jiangsu, P.R.China

*: Equal contribution authors

Corresponding Author:

Yang Hong

Department of Cell Biology

University of Pittsburgh School of Medicine

S325 BST, 3500 Terrace Street

Pittsburgh, PA 15261, USA

Phone: 412-648-2845

Fax: 412-648-8330

Email: yhong@pitt.edu; yang.hong@gmail.com

Running Title: Electrostatic plasma membrane targeting of Dlg

Keywords: Dlg, Lgl, Scrib, aPKC, Par-6, polybasic domain, phosphoinositides, PI4P, PI(4,5)P_2, cell polarity, tumorigenesis

SUMMARY (180 words)

Discs large (Dlg) is an essential polarity protein and a tumor suppressor originally characterized in *Drosophila* but is also well conserved in vertebrates. Like the majority of polarity proteins, plasma membrane (PM)/cortical localization of Dlg is required for its function in regulating apical-basal polarity and tumorigenesis, but the exact mechanisms targeting Dlg to PM remain to be unclear. Here we show that, similar to recently discovered polybasic polarity proteins such as Lgl and aPKC, Dlg also contains a positively charged polybasic domain that electrostatically binds the PM phosphoinositides PI4P and PI(4,5)P_2. Electrostatic targeting by the polybasic domain acts as the primary mechanism localizing Dlg to the PM in follicular and early embryonic epithelial cells, and is crucial for Dlg to regulate both polarity and tumorigenesis. The electrostatic PM targeting of Dlg is controlled by a potential phosphorylation-dependent allosteric regulation of its polybasic domain, and is specifically enhanced by interactions between Dlg and another basolateral polarity protein and tumor suppressor Scrib. Our studies highlight an increasingly significant role of electrostatic PM targeting of polarity proteins in regulating cell polarity.

INTRODUCTION:

Polarity proteins play conserved and essential roles in regulating the apical-basal polarity in epithelial cells of both invertebrates and vertebrates (Rodriguez-Boulan and Macara, 2014). Among the dozen or so polarity proteins, Discs large (Dlg), Scrib and Lgl, which were all originally characterized in *Drosophila*, also act as tumor suppressors and share the same basolateral subcellular localization in epithelial cells (Bilder et al., 2003; Tanentzapf and Tepass, 2003). Like many polarity proteins, the plasma membrane (PM)/cortical localization is essential for Dlg, Lgl and Scrib for regulating apical-basal polarity and tumorigenesis (Hough et al., 1997; Ventura et al., 2020). Recent studies have discovered that multiple polarity proteins contain so-called polybasic (PB) domains that are typically of 20-40aa length and highly positively charged due to the enrichment of Arg and Lys residues (Hammond and Hong, 2017). Polybasic (domain) polarity proteins like Lgl and aPKC can specifically target to PM by electrostatically binding the negatively charged phospholipids, in particular PI4P and $PI(4,5)P_2$ (PIP2) whose unique enrichment in PM makes the inner surface of PM the most negatively charged in the cell (Hammond and Hong, 2017; Hammond et al., 2012). While the electrostatic PM targeting of Lgl is now well established (Bailey and Prehoda, 2015; Dong et al., 2015), the exact mechanisms targeting Dlg to cell cortex or PM remain to be fully elucidated. Here we report that Dlg, like recently characterized polybasic polarity proteins Lgl and aPKC (Dong et al., 2020) contains a positively charged polybasic domain that targets Dlg to the PM and is necessary for Dlg to regulate polarity and tumorigenesis. Our results suggest that Scrib specifically enhances the electrostatic PM targeting of Dlg which is regulated by potential phosphorylation-dependent allosteric controls.

RESULTS AND DISCUSSION:

A polybasic domain in Dlg mediates its PM targeting in *Drosophila* epithelial cells

Dlg belongs to the MAGUK protein family and contains three PDZ domains, one SH3 domain, one HOOK domain and one guanylate kinase (GUK) domain (Fig. 1A). The GUK domain in MAGUK proteins is considered kinase dead and instead acts as a protein interacting domain which, in the case of Dlg, has the potential to bind SH3 domain either intramolecullarly or intermolecullarly (McGee et al., 2001) (see below). By sequence search we identified a well conserved candidate polybasic domain that spans the C-terminal half of SH3 and the N-terminal half of HOOK domains (Fig. 1A) and has a basic-hydrophobic index (Brzeska et al., 2010) of 0.90, comparable to polybasic domains in Lgl (1.01), aPKC (0.96), and Numb (1.07). In

liposome pull-down assays, GST fusion of wild type Dlg PB domain (GST-PB) bound both PI4P- and PIP2-liposomes but not liposomes containing only phosphatidylserine (PS) (Fig. 1A). GST-PB-KR6Q or GST-PB-KR15Q in which positive charges were either partially or completely eliminated by K/R->Q mutations did not bind either PI4P- or PIP2-liposomes (Fig. 1A), supporting an electrostatic interaction between the positively charged polybasic domain and negatively charged PI4P- or PIP2-membrane.

To investigate whether the PB domain is required for targeting Dlg to PM in vivo, we generated transgenic flies expressing Dlg::GFP, Dlg^{KR6Q}::GFP and Dlg^{KR15Q}::GFP under the ubiquitin promoter (Dong et al., 2020). Although *dlg* locus apparently expresses numerous isoforms, our Dlg::GFP based on isoform G fully rescued null mutants of *dlg*$^{[A]}$ (Haelterman et al., 2014; Ventura et al., 2020) and showed typical basolateral PM/cortex localization in follicular cells (Fig. 1C) and embryonic epithelial cells (Fig. S1A). In contrast, both Dlg^{KR6Q} and Dlg^{KR15Q} showed dramatically reduced PM localization (Fig. 1C, S1C) and failed to rescue *dlg*$^{[A]}$ (Table S1). Dlg interacts with multiple proteins on the PM through its three PDZ domains (Hough et al., 1997). Nonetheless, in follicular cells PM localization of Dlg$^{\Delta PDZ}$::GFP is comparable to Dlg::GFP, while Dlg$^{\Delta PDZ\text{-}KR6Q}$::GFP and Dlg$^{\Delta PDZ\text{-}KR15Q}$::GFP were virtually lost from PM (Fig. 1C), suggesting that PM targeting of Dlg in follicular cells is primarily mediated by the polybasic domain.

To further investigate the electrostatic PM targeting of Dlg in vivo, we used previously established hypoxia assays in which we acutely and reversibly deplete phospholipids PIP2 and PI4P in the PM (Dong et al., 2015) (data not shown). Similar to polybasic polarity proteins Lgl (Dong et al., 2015) and aPKC (Dong et al., 2020), in follicular cells hypoxia induced acute loss of PM Dlg::GFP which was reversed by subsequent reoxygenation (Fig. 1D). However, unlike Lgl which became completely cytosolic well within 30-60min of hypoxia, residual PM localization of Dlg::GFP persisted over 100min of hypoxia (Fig. 1D). In contrast, hypoxia induced complete loss of PM Dlg$^{\Delta PDZ}$::GFP identical to Lgl (Fig. 1D). Such data suggest that in follicular cells the majority of Dlg electrostatically binds PM, with PDZ domain-dependent interactions retaining a minor portion of Dlg on the PM.

Dlg is also a component of septate junction (SJ) which is composed of over twenty different proteins (Izumi and Furuse, 2014), making SJ the primary target of PDZ-dependent PM localization of Dlg. In early stage embryos which have not developed mature SJ, Dlg::GFP was readily lost from PM under hypoxia in embryonic epithelia cells, suggesting that PM targeting of Dlg is mostly electrostatic (Fig. S1A). In stage 14 or later embryos with mature SJ, PM localization of Dlg::GFP was significantly enhanced (Fig. S1C, D) and became fully resistant to

hypoxia (Fig. S1A). In contrast, in stage 14 embryos mutant of core SJ proteins such as Coracle (*cora*) (Lamb et al., 1998) or Na^+,K^+-ATPase α-subunit (*Atpα*) (Paul et al., 2003) PM Dlg::GFP remained sensitive to hypoxia (Fig. S1B). Notably, enhancement of PM localization in late stage embryos was also seen in Dlg mutants defective in electrostatic PM targeting, but not in mutants that lacking the PDZ domains (Fig. S1C, D), consistent with that PDZ domains are required for Dlg localization through SJ (Hough et al., 1997). Indeed, PM localization of $Dlg^{\Delta PDZ}$::GFP in stage 14 embryos appeared to be electrostatic based on its sensitivity to hypoxia (Fig. S1B).

In summary, with the help hypoxia-based imaging assays we were able to specifically probe the electrostatic PM targeting of Dlg in vivo. Our data confirm that in follicular and early embryonic epithelial cells electrostatic binding mediated by the polybasic domain is essential for Dlg PM targeting, although in late embryonic epithelial cells with mature SJ the PDZ domain-dependent interactions can act redundantly to retain Dlg on the PM.

PM targeting of Dlg depends on PI4P and PIP2 in vivo

PM phosphoinositides PI4P and PIP2 are majorly responsible for electrostatically binding polybasic domain proteins (Hammond, 2012). To investigate how PIP2 may be responsible for targeting Dlg in vivo, we used a previously established system to acutely deplete PIP2 (Dong et al., 2020; Dong et al., 2015; Reversi et al., 2014) in follicular cells. In this inducible system addition of rapamycin induces dimerization between a FRB-tagged PM anchor protein (i.e. Lck-FRB-CFP) and a FKBP-tagged phosphatase (i.e. RFP-FKBP-INPP5E), resulting in acute PM recruitment of INPP5E to rapidly deplete PM PIP2 (Reversi et al., 2014)(Hammond, 2012). For reasons unknown, the levels of PM Dlg::GFP or $Dlg^{\Delta PDZ}$::GFP were increased in cells expressing Lck-FRB and FKBP-INPP5E, regardless of DMSO or rapamycin treatment (Fig. 2A). Nonetheless, under rapamycin but not DMSO treatment, PM localization of both Dlg::GFP and $Dlg^{\Delta PDZ}$::GFP showed much strong reduction in cells expressing Lck-FRB and FKBP-INPP5E (Fig. 2A), supporting that the PM targeting of Dlg is at least partially dependent on PM PIP2.

At present, similar tools for acutely depleting PI4P or both PI4P and PIP2 are not available in *Drosophila*. To investigate how PI4P may be required for Dlg's PM targeting, we reduced its levels genetically by RNAi-knock down of PI4KIIIα, the PtdIns-4-kinase specifically responsible for maintaining the PM PI4P levels (Bojjireddy et al., 2014; Tan et al., 2014). Wild type cells and *PI4KIIIα-RNAi* cells showed similar levels of PM Dlg::GFP and $Dlg^{\Delta PDZ}$::GFP and losses under hypoxia (Fig. 2B). However, consistent with previous studies in cultured cells

suggesting that PI4KIIIα is necessary for replenishing PM PI4P and PIP2 (Bojjireddy et al., 2014), PM recoveries of Dlg::GFP and Dlg$^{\Delta PDZ}$::GFP were significantly delayed in *PI4KIIIα-RNAi* cells (Fig. 2B). Overall, our data suggest that PI4P and PIP2 likely act redundantly to electrostatically bind Dlg to PM.

Potential phosphorylation events on the PB domain regulates the PM targeting of Dlg

Polybasic domains are often regulated by direct phosphorylation which inhibit PM binding by neutralizing the positive charges (Hong, 2018), such as in the cases of polybasic polarity proteins Lgl, Numb and Miranda (Bailey and Prehoda, 2015; Dong et al., 2015). To investigate whether Dlg polybasic domain is also regulated by phosphorylation events, we mutated four previously characterized phosphorylation sites of aPKC and PKCα that are well conserved within the polybasic domain (Golub et al., 2017; O'Neill et al., 2011) (Fig. 1A). Interestingly, both phosphomemitic mutant Dlg^{S4D}::GFP and non-phosphorylatable mutant Dlg^{S4A}::GFP showed significant loss from PM (Fig. 3A), suggesting that the potential phosphorylation events on four serine residues unlikely regulate the PB domain through charge neutralization. PM Dlg^{S4A}::GFP, albeit reduced, was resistant to hypoxia (Fig. S2A), while removing PDZ domains in Dlg^{S4A}::GFP nearly abolished the PM localization of Dlg$^{\Delta PDZ\text{-}S4A}$::GFP (Fig. 3A). The data is consistent with that the residual PM localization of Dlg^{S4A}::GFP is non-electrostatic but PDZ domain-dependent, suggesting that the polybasic domain in Dlg^{S4A}::GFP is somehow blocked from binding to PM.

Recent studies also showed that the polybasic domain in aPKC, which is the pseudosubstrate region (PSr) with no characterized phosphorylation sites, is allosterically regulated (Dong et al., 2020). The PSr in aPKC binds and autoinhibits the kinase domain which in turn occludes PSr from electrostatically binding to PM, while binding of Par-6 to aPKC induces conformation changes exposing the PSr to PM-binding (Dong et al., 2020). Given that SH3 and GUK domains in Dlg could also bind each other either intra- or inter-molecularly, we postulate that loss of phosphorylation events in Dlg^{S4A}::GFP keeps the SH3-GUK in a closed conformation that occlude the polybasic domain from binding PM. Removing the GUK domain, however, made Dlg$^{\Delta GUK}$::GFP partially nuclear localized in addition to its PM localization (Fig. 3A). Given that the Arg/Lyn-rich feature of PB domain is similar to nuclear localization signal (NLS) domain, it appears that the polybasic domain in ΔGUK mutants is biased to nuclear localization for reasons presently unclear. Nonetheless, PM localization of Dlg$^{\Delta GUK}$::GFP is still electrostatic as it was sensitive to hypoxia (Fig. S2B). Dlg$^{S4A\text{-}\Delta GUK}$::GFP showed even more

enhanced nuclear localization, supporting that removing GUK helps to expose the polybasic domain in Dlg^{S4A}::GFP in the absence of phosphorylation events. Although more studies are needed, our results so far suggest that polybasic domain in Dlg may be allosterically regulated by its phosphorylation.

Scrib specifically enhances the electrostatic PM targeting of Dlg

Both Scrib and Lgl colocalize with Dlg at basolateral PM and play similar functions in regulating cell polarity and tumorigenesis, although regulatory relationships among three proteins have been rather complicated (Khoury and Bilder, 2020; Ventura et al., 2020). In particular, it is unknown how Scrib and Lgl may specifically regulate the electrostatic PM targeting of Dlg. Consistent with recent studies that Scrib but not Lgl appears to physically interact with Dlg, knocking down Scrib by RNAi induced a partial loss of Dlg from PM (Fig. 3B). More importantly, Scrib appears to specifically enhance the electrostatic PM targeting of Dlg, as Dlg$^{\Delta PDZ}$::GFP, which can only bind PM electrostatically, was dramatically lost from PM in *scrib-RNAi* cells (Fig. 3B). In contrast, the residual PM localization of electrostatic targeting mutant Dlg^{KR6Q}::GFP was not affected by *scrib-RNAi* (Fig. 3B). It was reported that Scrib interacts specifically with the SH3 domain in Dlg and a single point mutation in SH3 domain found in *dlg^{m30}* mutant (Fig.1A) abolishes the physical interaction between the two proteins (Khoury and Bilder, 2020). Indeed, similar to electrostatic mutants such as Dlg^{KR6Q}::GFP, Dlg^{S4A}::GFP or Dlg$^{\Delta GUK}$::GFP, PM Dlg^{m30}::GFP was also reduced and was not affected by *scrib-RNAi* (Fig. 3B), suggesting that the physical interaction between Scrib and Dlg is required for Scrib to enhance the electrostatic PM targeting of Dlg. Interestingly, PM Dlg^{S4A}::GFP or Dlg$^{\Delta GUK}$::GFP was also resistant to *scrib-RNAi* (Fig. 3B), suggesting that Scrib may act through the phosphorylation-dependent conformation changes that expose the Dlg polybasic domain to bind PM.

Finally, in agreement with the recent findings that Lgl does not appear to physically associate with Dlg and Scrib (Khoury and Bilder, 2020; Ventura et al., 2020), *lgl-RNAi* did not affect the PM localization of Dlg, Dlg^{KR6Q}, Dlg^{S4A}, Dlg^{m30} and Dlg$^{\Delta GUK}$ (Fig. 3C). However, PM localization of Dlg$^{\Delta PDZ}$::GFP was mildly reduced in *lgl-RNAi* cells, suggesting that Lgl may still a moderate but specific role in enhancing the electrostatic PM targeting of Dlg (Fig. 3C).

Electrostatic PM targeting is essential for Dlg to regulate cell polarity and tumorigenesis

We also investigated how electrostatic PM targeting may specifically contribute to Dlg function in polarity and tumorigenesis. Follicular cells of *dlg*$^{-/-}$ showed dramatic disruption of cell polarity evidenced by the mislocalization of apical polarity protein such as aPKC (Fig. 4A). Such phenotype was fully rescued by ectopic expression of Dlg::GFP and Dlg$^{\Delta PDZ}$::GFP, but not electrostatic targeting mutant Dlg^{KR6Q}::GFP or Dlg$^{\Delta PDZ\text{-}KR6Q}$::GFP (Fig. 4A), suggesting that electrostatic PM targeting is essential for Dlg to regulate apical-basal polarity. Surprisingly, *dlg*$^{[A]}$*/Y; ubi-dlg*^{S4A}*::GFP* and *dlg*$^{[A]}$*/Y; ubi-dlg*$^{\Delta GUK}$*::GFP* males are viable although sterile (Table S1), suggesting that the potential mechanisms regulating the polybasic domain may be largely dispensable for Dlg during normal development.

To investigate how electrostatic PM targeting is required for Dlg's tumor suppressor function, we used a well-established fly tumor model (Brumby et al., 2011). Overexpression of constitutively active Ras^{V12} in larval eye disc yields a moderate rough eye phenotype due to mild cell overproliferation (Fig. 4B). While *dlg-RNAi* alone in the eye did not produce obvious phenotypes, combining Ras^{V12} over-expression and *dlg-RNAi* (i.e. "*Ras*^{V12}*/dlg-RNA*i") produced massive eye tumors which resulted in strong larval/pupal lethality, with very few surviving adults showing deformed eyes of much reduced sizes and with dark tumor tissues (Fig. 4B). We made transgenic stocks that express wild type or mutant Dlg proteins from cDNA sequences that were modified to be resistant to *dlg-RNAi* (Fig. S3, Table S2). Any of the ΔPDZ mutants is also resistant to *dlg-RNAi* as the RNAi targets the sequence near the N-terminal coding region. As expected, expression of RNAi-resistant Dlg::GFP ("Dlg^{R}::GFP") fully rescued lethality and eye morphology caused by *Ras*^{V12}*/dlg-RNA*i (Fig. 4B). Both Dlg$^{\Delta PDZ}$::GFP and polybasic mutant Dlg$^{KR6Q\text{-}R}$::GFP rescued lethality of *Ras*^{V12}*/dlg-RNAi*, but eyes in *dlg*$^{KR6Q\text{-}R}$*::GFP*-rescued flies still showed strong tissue overproliferation (Fig. 4B). In contrast, Dlg$^{\Delta PDZ\text{-}KR6Q}$::GFP failed to rescue either lethality or the eye morphology and tumorigenesis in *Ras*^{V12}*/dlg-RNAi* flies (Fig. 4B). Such data suggest that the tumor suppressor function of Dlg requires both electrostatic and PDZ domain-dependent PM targeting, with electrostatic PM targeting appears to be more specifically required for inhibiting the overproliferation of *Ras*^{V12}*/dlg-RNAi* tumor cells.

Notably, Dlg$^{m30\text{-}\Delta GUK}$::GFP, but not Dlg^{m30}::GFP or Dlg$^{m30\text{-}\Delta PDZ}$::GFP, partially rescued the polarity defects in *dlg*$^{-/-}$ cells (Fig. 4A). RNAi-resistant Dlg$^{m30\text{-}R}$::GFP only moderately rescued the lethality by *Ras*^{V12}*/dlg-RNAi*, and survivors still suffered strong overproliferation in eyes (Fig. 4B). Consistent with the polarity rescue results in Fig. 4A, removing GUK but not PDZ domains in Dlg^{m30} significantly rescued the overproliferation phenotype in Ras^{V12}*/dlg-RNAi* eyes (Fig. 4B). Such data suggest that loss of Scrib-dependent enhancement of Dlg electrostatic PM targeting

can be partially compensated by eliminating the potential allosteric regulation of polybasic domain in Dlg.

The electrostatic nature of the Dlg PM targeting shown in this study makes Dlg a new member of the polybasic polarity protein family which includes at least Lgl, aPKC, Numb and Miranda. Our results also make it increasingly clear that electrostatic PM binding is a key molecular mechanism widely used by the polarity proteins for achieving controlled subcellular localization and for regulating cell polarity. It will be of great interest for future studies to further integrate the electrostatic PM targeting mechanism into the regulatory network of polarity protein and their interacting partners, by uncovering the essential molecular mechanisms that regulate this simple but elegant physical interaction between polarity proteins and PM.

Acknowledgements

We are grateful to Drs. David Bilder, Helena Richardson, Greg Beitel, Richard Fehon, Ulli Tepass, and Stefano De Renzis for reagents and fly stocks, Dr. Simon Watkins and University of Pittsburgh Medical School Center for Biologic Imaging for generous imaging and microscopy support, Bloomington Stock Center for fly stocks, and Developmental Studies Hybridoma Bank (DSHB) for antibodies.

Competing Interests

The authors declare no competing or financial interests.

Author Contributions

Conceptualization: Y.H., W.D. J.L.; Investigation: J.L, W.D., Y.T., Y.H.; Writing - Review &Editing: Y.H; Funding acquisition: Y.H.; Supervision: Y.H.

Funding

This work was supported by grants NIH- NCRR R21RR024869 (Y.H.), NIH-NIGMS R01GM086423 and R01GM121534 (Y.H.). University of Pittsburgh Medical School Center for

Biologic Imaging is supported by grant 1S10OD019973-01 from NIH.

MATERIALS AND METHODS

Fly Stocks: Flies of carrying transgenic *ubi-dlg::GFP* or *ubi-dlg::GFP* mutant ("*ubi-dlg**::GFP*") alleles were generated by *phiC31*-mediated integration protocol (Huang et al., 2009). *attP*^{VK00022} (BL#24868) stock was used to integrate *ubi-dlg:GFP* and *ubi-dlg**::GFP* constructs to the 2nd chromosome. Transgenic alleles of *ubi-dlg::GFP* and *ubi-dlg**::GFP* were further recombined with *y w dlg*$^{[A]}$ *FRT19A/FM7c* (BL#57086). Summary of *ubi-dlg**::GFP* alleles are in Table S1.

cora^{5} */ CyO dfdGMR-YFP and Atpα*^{DTS2A3} */ TM6 dfdGMR-YFP* are gifts from Dr. Greg Beitel, (Northwestern University, USA).

w UASp>mRFP::FKBP-5Ptase ("FKBP-INPP5E") and *w; ; UASp>Lck-FRB::CFP* are gifts from Dr. Stefano De Renzis (EMBL Heidelberg, Germany) (Reversi et al., 2014).

ey-Gal4, UAS-Ras^{V12} stocks were gift from Dr. Helena Richardson.

w P[w[+mC]=PTT-GC]dlg1$^{[YC0005]}$ *("dlg::GFP",* BL#50859*), UAS-PI4KIIIα-RNAi* (BL#35256), *UAS-scrib-RNAi* (BL#29552), *UAS-lgl-RNAi* (BL#38989), *UAS-dlg-RNAi* (II) (BL#39035) and *UAS-dlg-RNAi* (III) (BL#34854) are from Bloomington Stock Center.

w; lgl::mCherry knock-in stock was previously published (Dong et al., 2015).

Drosophila cultures and genetic crosses are carried out at 25ºC.

Molecular cloning. To make *ubi-dlg::GFP*, ubiquitin promoter (1872bp) was PCR amplified from plasmid pWUM6 (a gift from Dr. Jeff Sekelsky, University of North Carolina at Chapel Hill) using primers 5-AGTGTC GAATTC CGCGCAGATC GCCGATGGGC and 5-CTGGAC GCGGCCGC GGTGGATTATTCTGCGGG and inserted into pGE-attB vector (Huang et al., 2009) to generate vector pGU. DNA fragments encoding Dlg::GFP was then inserted into pGU vector. More details about DNA constructs used in this report are listed in Table S2. Sequence of the Dlg isoform used in this study can be found by NCBI RefSeq ID NP_996405.1.

Liposome pull-down assays. Liposomal binding assays were carried out as described (Kim et al., 2008). Lipid mixture of 37.5% PC (Cat#840051C), 10% PS (Cat#840032C), 37.5% PE (Cat#840021C), 10% Cholesterol (Cat#700000P) and 5% PI(4,5)P_2 (Cat#840046X) or PI4P (Cat#840045X, all lipids were purchased from Avanti Polar Lipids Inc) was dried and

resuspended to a final concentration of 1 mg/ml of total phospholipids in HEPES buffer and subjected to 30 min sonication. Formed liposomes were harvested at 16,000g for 10 min and resuspended in binding buffer (HEPES, 20 mM, 7.4, KCl 120 mM, NaCl 20mM, EGTA 1mM, MgCl 1mM BSA 1mg/ml). Approximately 0.1µg of purified protein or protein complex was mixed with 50µl of liposome suspension in each liposome-binding assay. Liposomes were pelleted at 16,000g for 10min after 15min incubation at room temperature, and were analyzed by western blot to detect co-sediment of target protein(s).

Generation of mitotic mutant clones in *Drosophila* follicular epithelia: Mutant follicular cell clones of *dlg*$^{[A]}$ were generated by the routine FLP/FRT technique. Young females were heat-shocked at 37°C for 1 hour and their ovaries were dissected 3 days later.

Live imaging and hypoxia treatment in *Drosophila* epithelial cells. Embryos and dissected ovaries were imaged according to previously published protocol (Dong et al., 2015; Huang et al., 2011). The embryos were staged by timing and kept in 25 °C for 2 hours before imaging. Ovaries from adult females of 2-days old were dissected in halocarbon oil (#95). Follicular cells containing over-expressing or RNAi clones were generated by heat-shocking the young females of the correct genotype at 37°C for 15-30min and ovaries were dissected 3 days later. To ensures sufficient air exchange to samples during the imaging session, dechorionated embryos or dissected ovaries were mounted in halocarbon oil on an air-permeable membrane (YSI Membrane Model #5793, YSI Inc, Yellow Springs, OH) sealed by vacuum grease on a custom-made plastic slide over a 10x10mm^2 cut-through window. The slide was then mounted in a custom made air-tight micro chamber for live imaging under confocal microscope. Oxygen levels inside the chamber were controlled by flow of either air or custom O_2/N_2 gas mixture at the rate of approximately 1-5 cc/sec. Images were captured at room temperature (25°C) on an Olympus FV1000 confocal microscope (60x Uplan FL N oil objective, NA=1.3) by Olympus FV10-ASW software, or on a Nikon A1 confocal microscope (Plan Fluo 60x oil objective, NA=1.3) by NIS-Elements AR software. Images were further processed in ImageJ and Adobe Photoshop.

Induction of mRFP::FKBP-5Ptase and Lck-FRB::CFP dimerization in live *Drosophila*

follicular cells. Young females of *w UASp>mRFP::FKBP-5Ptase /dlg::GFP;;hs-FLP Act5C(FRT.CD2)-Gal4 UAS-RFP/UASp>Lck-FRB::CFP* or *w UASp>mRFP::FKBP-5Ptase /+; ubi-dlg$^{\Delta PDZ}$::GFP/+; hs-FLP Act5C(FRT.CD2)-Gal4 UAS-RFP/UASp>Lck-FRB::CFP* were heat-shocked at 37°C for 15min. Ovaries were dissected 3 days later in Schneider's medium, mounted in a drop of 20µl Schneider's medium containing 10µM rapamycin or DMSO on a gas-permeable slide, and imaged live as previously described (Dong et al., 2015; Huang et al., 2011).

Immunostaining and confocal imaging: Immunostaining of follicular cells and embryos were carried out as previously described (Huang et al., 2009). Primary antibodies: chicken anti-GFP (Aves Lab, cat# GFP-1010) 1:5000; mouse anti-Dlg (DSHB, 4F3) 1:50; rabbit anti-aPKC (Santa Cruz, Sc-216) 1:1000. Secondary antibodies: Cy2- , Cy3 or Cy5-conjugated goat anti-rabbit IgG, anti-mouse IgG, and anti-chicken IgG (The Jackson ImmunoResearch Lab, 111-225-003, 115-165-003, and 106-175-003), all at 1:400. Images were collected on Olympus FV1000 confocal microscopes (Center for Biologic Imaging, University of Pittsburgh Medical School) and processed in Adobe Photoshop for compositions.

Image Processing and Quantification: Time-lapse movies were first stabilized by HyperStackReg plug-in in ImageJ. Images or movies containing excessive noisy channels were denoised by PureDenoise plugin in ImageJ prior to quantification. PM localization of GFP or RFP in images or movies were measured in Image J by custom macro scripts. In each image or the first frame of the movie, ROIs approximately 20-40µm^2 were drawn across selected cell junctions. In most cases, custom macros was used to automatically generate PM masks by threshold-segmentation that was based on the mean pixel value of the ROI. Custom macros were then used to automatically measure PM and cytosolic intensities of each fluorescent protein in ROIs in an image or throughout all the frames of a movie. Backgrounds were manually measured based on the minimal pixel value of the whole image or the first frame of the movie. The PM localization index for each fluorescent protein was auto-calculated by the macro as the ratio of [PM - background]/[cytosol - background]. In live imaging experiments, "Normalized PM Index" was calculated by normalizing (PM Index -1) over the period of recording against the (PM Index -1) at 0 minute. Data were further processed in Excel, visualized and analyzed in Graphpad Prism.

Tumorigenesis assays: RNAi-resistance wild type or mutant *ubi-dlg::GFP* ("*dlg^{R**}::GFP*") transgenic alleles were crossed with *ey-Gal4 UAS-Ras^{V12}/CyO-Gal80; UAS-dlg-RNAi/TM6B* and crosses were transferred to a new viral every 3-4 days. F1 progenies from each cross were scored into two groups based on their genotypes: *dlg^{R**}::GFP /ey-Gal UAS-Ras^{V12}; UAS-dlg-RNAi/+* (group#1) or *dlg^{R**}::GFP /ey-Gal UAS-Ras^{V12}; TM6B/+* (group#2). The ratio between groups #1 and #2 were calculated as "Rescue" index for each *dlg^{R**}::GFP* allele. Representative eyes of flies from group#1 were imaged.

FIGURE LEGENDS

Figure 1. A polybasic domain in Dlg mediates its electrostatic PM targeting.

(**A**) Sequences of polybasic domains in human Dlg1 (hDlg1, NP_004078.2) and *Drosophila* Dlg (NP_996405). Mutations made in Dlg^{KR6Q}, Dlg^{KR15Q} and Dlg^{S4A}, as well as the point mutation of dlg^{m30} ("*m30*") allele, are also shown. Deletions made in $Dlg^{\Delta PDZ}$ and $Dlg^{\Delta GUK}$ are illustrated at the bottom.

(**B**) Western blot by GST antibody showed that GST-PB, but not GST or GST-PB-KR6Q or GST-PB-KR15Q, co-sedimented with PI4P- and PIP2-liposomes. GST-PB did not bind to liposomes containing only 10% PS.

(**C**) Quantifications and representative images of PM localization of wild type and mutant Dlg::GFP in follicular cells. PM Index: values above 1 (dashed line) indicate predominant PM localization while below 1 indicate cytosolic localization. In parentheses: sample numbers (*n*).

(**D, E**) Selected frames from time-lapse recordings of follicular cells expressing Dlg::GFP and Lgl::mCherry (D, Movie S1) or $Dlg^{\Delta PDZ}$::GFP and Lgl::mCherry (E, Movie S2) undergoing hypoxia followed by reoxygenation. Quantification of PM localizations of Dlg and Lgl are shown in D' (*n*=20) and E' (*n*=20). Kymographs of PM Dlg/Lgl and $Dlg^{\Delta PDZ}$/Lgl were sampled at the boxes indicated in D and E, generated by maximum projection and colored in Fire-LUT in ImageJ. Arrowheads in kymographs highlighting the persistent residual PM Dlg under hypoxia. Time stamps in *hh:mm:ss* format.

Figure 2. Electrostatic PM targeting of Dlg depends on PI4P and PIP2.

(**A**). *dlg::GFP* or $dlg^{\Delta PDZ}$*::GFP* follicular epithelia were treated with either DMSO (control) or rapamycin ("rapa(+)") and imaged live. Cells expressing Lck-FRB-CFP (not imaged) and RFP-FKBP-INPP5E ("INPP5E") were labeled by nuclear RFP. (**A'**) Quantification of PM Dlg::GFP or $Dlg^{\Delta PDZ}$::GFP in wild type cells (green dots) and INPP5E cells (red dots) in both DMSO and rapa(+) samples. In parentheses: sample numbers.

(**B, C**). Selected frames of time-lapse recordings of follicular cells expressing Dlg::GFP (B, Movie S3) or $Dlg^{\Delta PDZ}$::GFP (C, Movie S4) undergoing hypoxia and reoxygenation. Cells expressing *PI4KIIIα-RNAi* were labeled by RFP. (**B', C'**) Quantification of PM Dlg::GFP (B') or $Dlg^{\Delta PDZ}$::GFP (C') in both wild type (green lines) and *PI4KIIIα-RNAi* (red lines) cells (*n*=20 for

each quantifications).

Time stamps in *hh:mm:ss* format.

Figure 3. Scrib enhances the electrostatic PM targeting of Dlg.

(**A**) Representative images of follicular cells expressing GFP-tagged Dlg mutants as indicated. PM localization of each mutant was quantified in A'.

(**B, C**) Representative images of follicular cells expressing wild type and mutant Dlg::GFP as indicated. Cells expressing *scrib-RNAi* (**B**) or *lgl-RNAi* (**C**) were labeled by RFP. PM localizations of wild type and mutant Dlg::GFP in wild type (green dots) and *RNAi* (red dots) cells were quantified in **B'** and **C.**

In parentheses: sample numbers.

****: p<0.00001. *ns*: p>0.05.

Figure 4. Electrostatic PM targeting of Dlg regulates cell polarity and tumorigenesis.

(**A**) Representative immunostaining images of follicular cells containing $dlg^{-/-}$ clones marked by loss of RFP (colored in blue in all merged images), except for the control "$dlg^{-/-}$ *wt*" in which the $dlg^{-/-}$ clones were marked with the absence of Dlg (green). All other samples expressed wild type or mutant Dlg::GFP as indicated. All samples were stained with anti-GFP (green) and anit-aPKC (red) antibodies. "*m30*": dlg^{m30}*::GFP*; "*m30-ΔPDZ*": $dlg^{m30\text{-}\Delta PDZ}$*::GFP*, "*m30-ΔGUK*": $dlg^{m30\text{-}\Delta GUK}$*::GFP*. Note that $dlg^{-/-}$, $dlg^{m30\text{-}\Delta GUK}$*::GFP* clones showed roughly equal frequency of rescued and non-rescued polarity defects. Asterisks highlight $dlg^{-/-}$ mutant cells.

(**B**) Representative images of eyes from adult flies of *ey-Gal4, UAS-*Ras^{V12} ("Ras^{V12}"), *ey-Gal4, UAS-dlg-RNAi* ("*dlg-RNAi*") or from flies of *ey-Gal4, UAS-*Ras^{V12}*, UAS-dlg-RNAi* ("Ras^{V12} *+ dlg-RNAi*") in combination with additional expression of wild type and mutant Dlg::GFP as indicated. "*ctrl*": Ras^{V12}*/dlg-RNAi* only.

(**C**) Quantifications of rescues of Ras^{V12}*/dlg-RNAi* lethality by wild type and mutant Dlg::GFP as indicated.

Figure 1

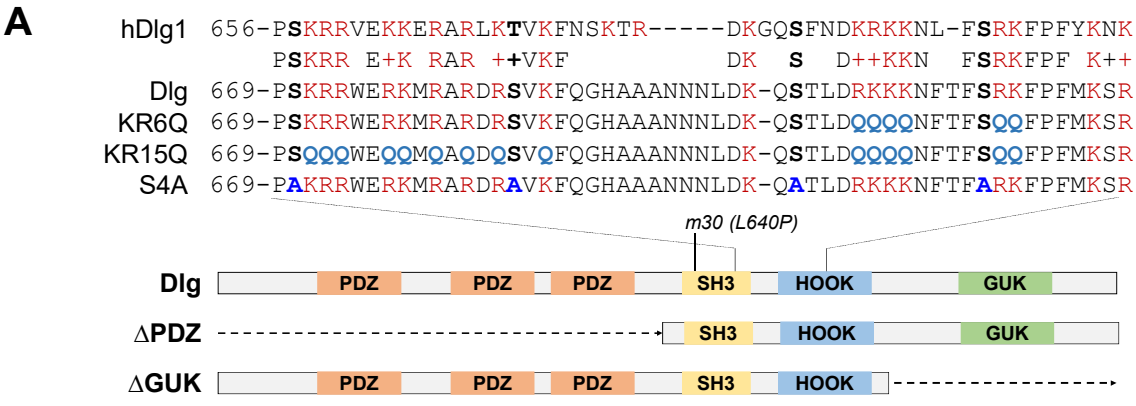

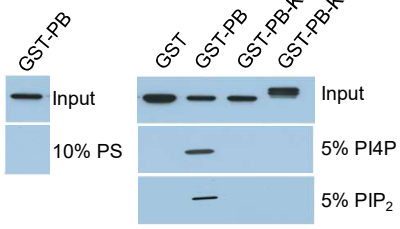

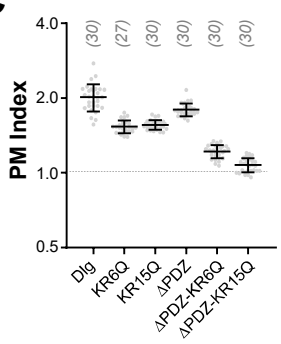

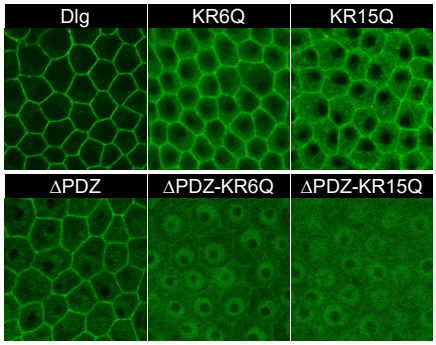

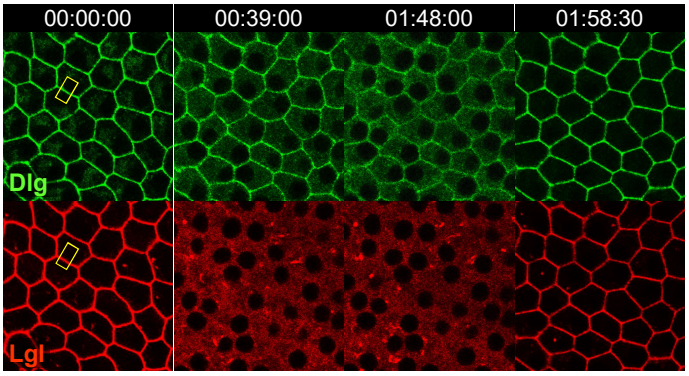

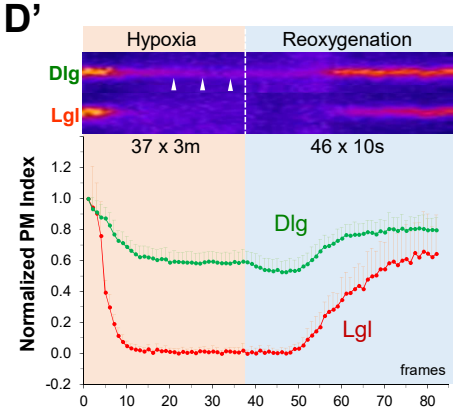

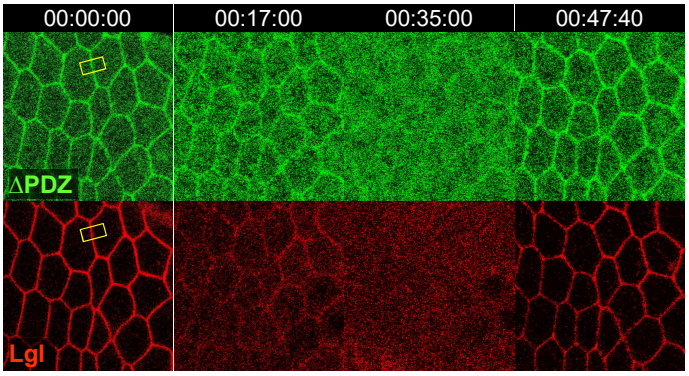

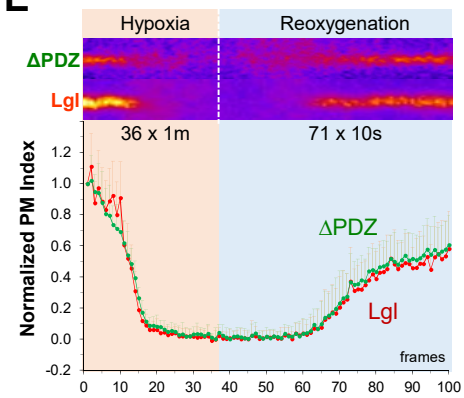

Figure 2

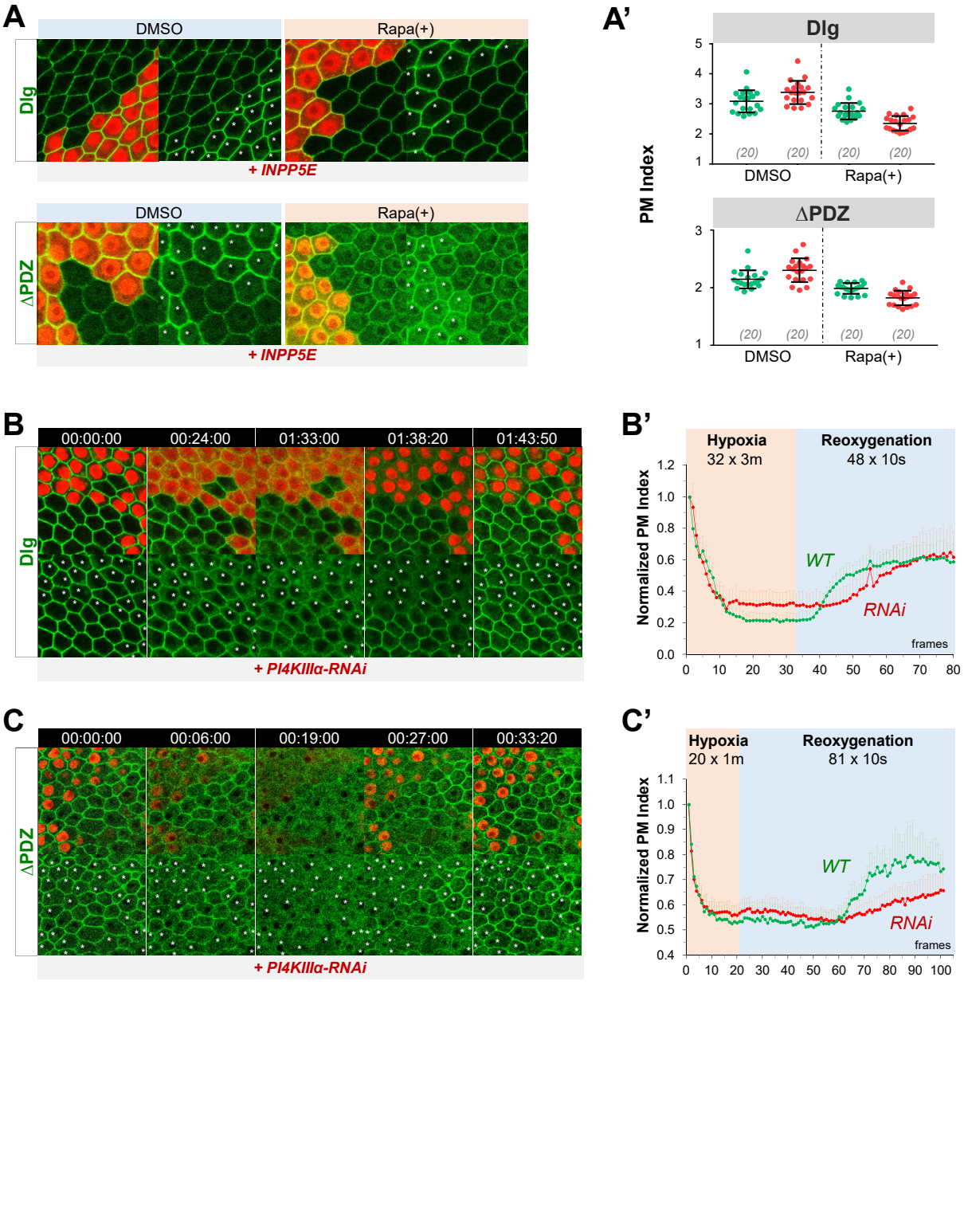

Figure 3

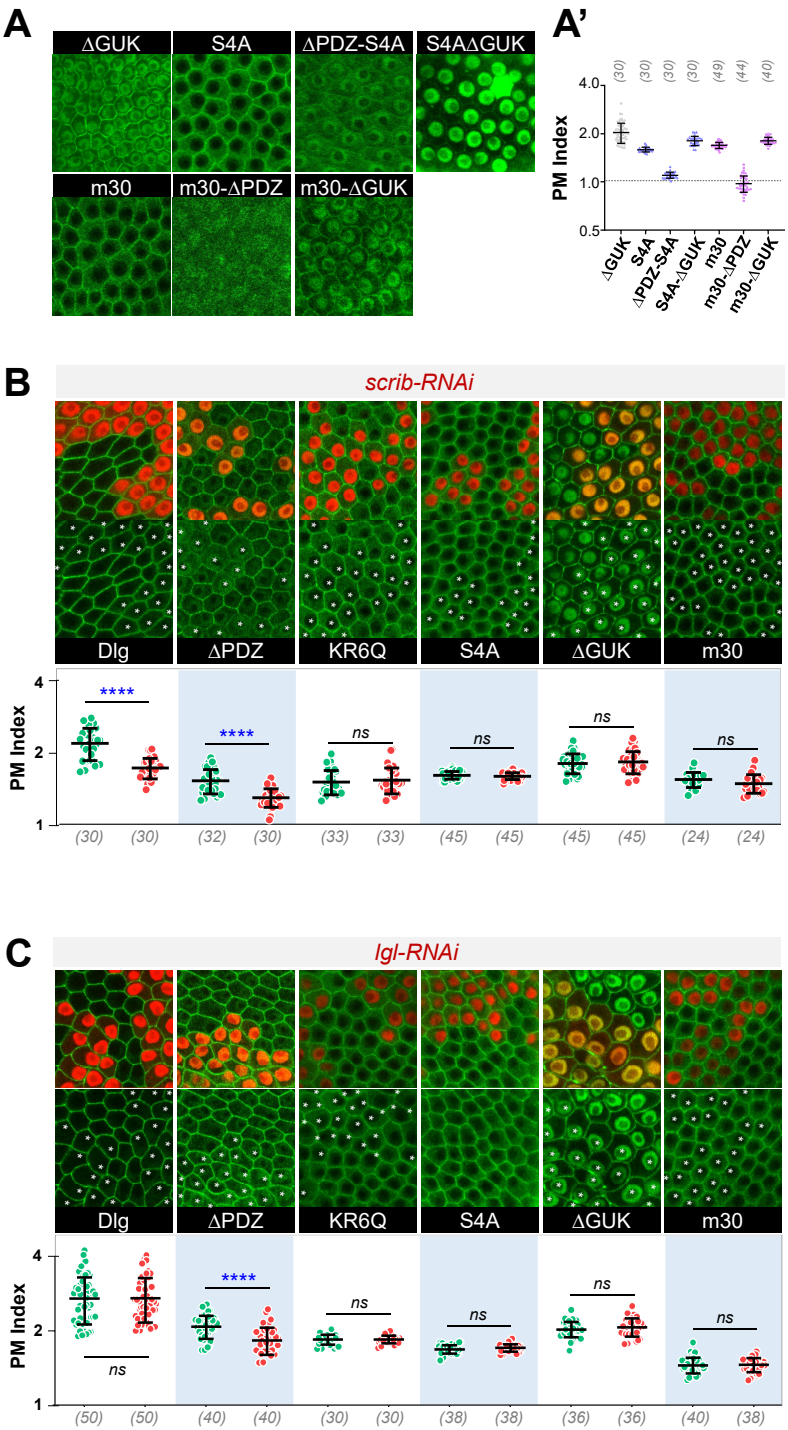

Figure 4

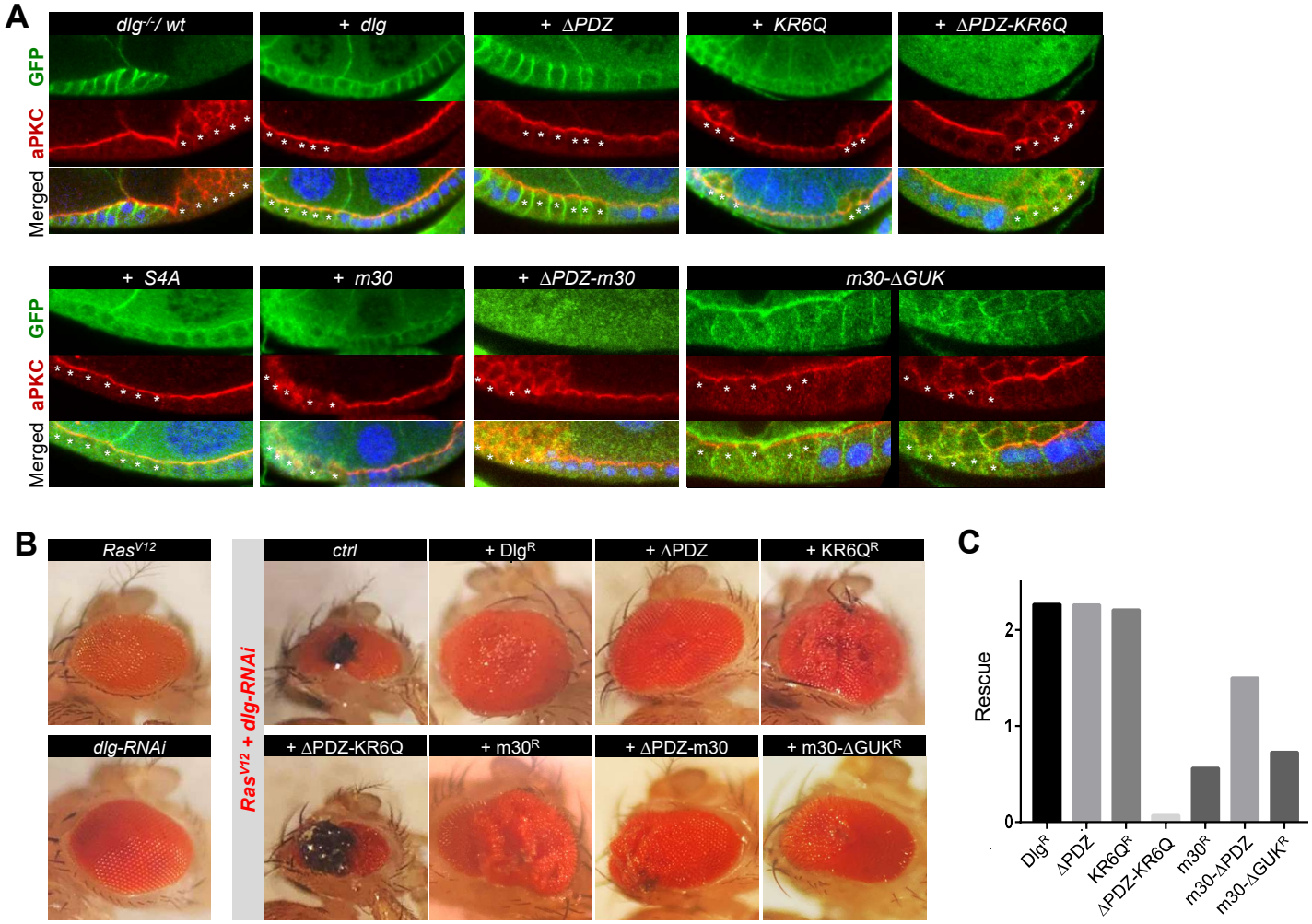

REFERENCES:

Bailey, Matthew J., Prehoda, Kenneth E., 2015. Establishment of Par-Polarized Cortical Domains via Phosphoregulated Membrane Motifs. Developmental Cell 35, 199-210.

Bilder, D., Schober, M., Perrimon, N., 2003. Integrated activity of PDZ protein complexes regulates epithelial polarity. Nat Cell Biol 5, 53-58.

Bojjireddy, N., Botyanszki, J., Hammond, G., Creech, D., Peterson, R., Kemp, D.C., Snead, M., Brown, R., Morrison, A., Wilson, S., Harrison, S., Moore, C., Balla, T., 2014. Pharmacological and Genetic Targeting of the PI4KA Enzyme Reveals Its Important Role in Maintaining Plasma Membrane Phosphatidylinositol 4-Phosphate and Phosphatidylinositol 4,5-Bisphosphate Levels. Journal of Biological Chemistry 289, 6120-6132.

Brumby, A.M., Goulding, K.R., Schlosser, T., Loi, S., Galea, R., Khoo, P., Bolden, J.E., Aigaki, T., Humbert, P.O., Richardson, H.E., 2011. Identification of Novel Ras-Cooperating Oncogenes in *Drosophila* melanogaster: A RhoGEF/Rho-Family/JNK Pathway Is a Central Driver of Tumorigenesis. Genetics 188, 105-125.

Brzeska, H., Guag, J., Remmert, K., Chacko, S., Korn, E.D., 2010. An Experimentally Based Computer Search Identifies Unstructured Membrane-binding Sites in Proteins: APPLICATION TO CLASS I MYOSINS, PAKS, AND CARMIL. Journal of Biological Chemistry 285, 5738-5747.

Dong, W., Lu, J., Zhang, X., Wu, Y., Lettieri, K., Hammond, G.R., Hong, Y., 2020. A polybasic domain in aPKC mediates Par6-dependent control of membrane targeting and kinase activity. Journal of Cell Biology 219.

Dong, W., Zhang, X., Liu, W., Chen, Y.-j., Huang, J., Austin, E., Celotto, A.M., Jiang, W.Z., Palladino, M.J., Jiang, Y., Hammond, G.R.V., Hong, Y., 2015. A conserved polybasic domain mediates plasma membrane targeting of Lgl and its regulation by hypoxia. The Journal of Cell Biology 211, 273-286.

Golub, O., Wee, B., Newman, R.A., Paterson, N.M., Prehoda, K.E., 2017. Activation of Discs large by aPKC aligns the mitotic spindle to the polarity axis during asymmetric cell division. eLife 6, e32137.

Haelterman, N.A., Jiang, L., Li, Y., Bayat, V., Sandoval, H., Ugur, B., Tan, K.L., Zhang, K., Bei, D., Xiong, B., Charng, W.-L., Busby, T., Jawaid, A., David, G., Jaiswal, M., Venken, K.J.T., Yamamoto, S., Chen, R., Bellen, H.J., 2014. Large-scale identification of chemically induced mutations in *Drosophila* melanogaster. Genome Research 24, 1707-1718.

Hammond, G.R., Hong, Y., 2017. Phosphoinositides and Membrane Targeting in Cell Polarity. Cold Spring Harbor Perspectives in Biology.

Hammond, G.R.V., Fischer, M.J., Anderson, K.E., Holdich, J., Koteci, A., Balla, T., Irvine, R.F., 2012. PI4P and PI(4,5)P2 Are Essential But Independent Lipid Determinants of Membrane Identity. Science 337, 727-730.

Hong, Y., 2018. aPKC: the Kinase that Phosphorylates Cell Polarity. F1000Research 7.

Hough, C.D., Woods, D.F., Park, S., Bryant, P.J., 1997. Organizing a functional junctional complex requires specific domains of the *Drosophila* MAGUK Discs large. Genes Dev 11, 3242-3253.

Huang, J., Huang, L., Chen, Y.-J., Austin, E., Devor, C.E., Roegiers, F., Hong, Y., 2011. Differential regulation of adherens junction dynamics during apical-basal polarization. J Cell Sci 124, 4001-4013.

Huang, J., Zhou, W., Dong, W., Watson, A.M., Hong, Y., 2009. Directed, efficient, and versatile modifications of the *Drosophila* genome by genomic engineering. Proc Natl Acad Sci U S A 106, 8284-8289.

Izumi, Y., Furuse, M., 2014. Molecular organization and function of invertebrate occluding junctions. Semin Cell Dev Biol 36, 186-193.

Khoury, M.J., Bilder, D., 2020. Distinct activities of Scrib module proteins organize epithelial polarity. Proceedings of the National Academy of Sciences, 201918462.

Kim, A.Y., Tang, Z., Liu, Q., Patel, K.N., Maag, D., Geng, Y., Dong, X., 2008. Pirt, a Phosphoinositide-Binding Protein, Functions as a Regulatory Subunit of TRPV1. Cell 133, 475-485.
Lamb, R.S., Ward, R.E., Schweizer, L., Fehon, R.G., 1998. *Drosophila* coracle, a Member of the Protein 4.1 superfamily, Has Essential Structural Functions in the Septate Junctions and Developmental Functions in Embryonic and Adult Epithelial Cells. Mol Biol Cell 9, 3505-3519.
McGee, A.W., Dakoji, S.R., Olsen, O., Bredt, D.S., Lim, W.A., Prehoda, K.E., 2001. Structure of the SH3-Guanylate Kinase Module from PSD-95 Suggests a Mechanism for Regulated Assembly of MAGUK Scaffolding Proteins. Molecular Cell 8, 1291-1301.
O'Neill, A.K., Gallegos, L.L., Justilien, V., Garcia, E.L., Leitges, M., Fields, A.P., Hall, R.A., Newton, A.C., 2011. Protein Kinase Cα Promotes Cell Migration through a PDZ-Dependent Interaction with its Novel Substrate Discs Large Homolog 1 (DLG1). Journal of Biological Chemistry 286, 43559-43568.
Paul, S.M., Ternet, M., Salvaterra, P.M., Beitel, G.J., 2003. The Na⁺/K⁺ ATPase is required for septate junction function and epithelial tube-size control in the *Drosophila* tracheal system. Development 130, 4963-4974.
Reversi, A., Loeser, E., Subramanian, D., Schultz, C., De Renzis, S., 2014. Plasma membrane phosphoinositide balance regulates cell shape during *Drosophila* embryo morphogenesis. The Journal of Cell Biology 205, 395-408.
Rodriguez-Boulan, E., Macara, I.G., 2014. Organization and execution of the epithelial polarity programme. Nat Rev Mol Cell Biol 15, 225-242.
Tan, J., Oh, K., Burgess, J., Hipfner, D.R., Brill, J.A., 2014. PI4KIIIalpha is required for cortical integrity and cell polarity during *Drosophila* oogenesis. J Cell Sci 127, 954-966.
Tanentzapf, G., Tepass, U., 2003. Interactions between the crumbs, lethal giant larvae and bazooka pathways in epithelial polarization. Nat Cell Biol 5, 46-52.
Ventura, G., Moreira, S., Barros-Carvalho, A., Osswald, M., Morais-de-Sá, E., 2020. Lgl cortical dynamics are independent of binding to the Scrib-Dlg complex but require Dlg-dependent restriction of aPKC. Development 147, dev186593.

SUPPLEMNTARY INFORMATION

SUPPLEMNTARY TABLES:

Table S1. Genetic Rescue Analyses of *dlg::GFP* Transgenic Alleles.

Genotype	Rescue of *dlg-/-*	Polarity Rescue	Tumor Rescue	Loclization
ubi-dlg::GFP	Y	Y	Y	PM
*ubi-dlg-**KR6Q**::GFP*	N	N	N	PM/Cyto
*ubi-dlg-**KR15Q**::GFP*	N	-	N	PM/Cyto
*ubi-dlg-Δ**PDZ**::GFP*	N	Y	Y	PM/Cyto
*ubi-dlg-Δ**PDZ-KR6Q**::GFP*	-	N	N	Cyto
*ubi-dlg-Δ**PDZ-KR15Q**::GFP*	-	N	N	Cyto
*ubi-dlg-Δ**GUK**::GFP*	Y*	Y	Y	PM/Nuc
*ubi-dlg-**S4A**::GFP*	Y*	Y	Y	PM/Cyto
*ubi-dlg-Δ**PDZ-S4A**::GFP*	-	Y	Y	Cyto
*ubi-dlg-**S4A-**Δ**GUK**::GFP*	-	-	N	Nuc/PM
*ubi-dlg-**m30**::GFP*	N	N	N	PM/Cyto
*ubi-dlg-Δ**PDZ-m30**::GFP*	-	N	N	Cyto
*ubi-dlg-**m30-**Δ**GUK**::GFP*	-	*partial*	*partial*	PM/Nuc

*: sterile

Nuc: nuclear

Cyto: cytosolic

PM: plasma membrane

-: not done.

Table S2. *dlg::GFP* Transgenic Alleles.

Construct	Vector	Description
Dlg::GFP	pGU::GFP	Full length Dlg inserted into pGU::GFP
Dlg-KR6Q::GFP	pGU::GFP	Dlg::GFP with 6 Lys/Arg residues in PB mutated to Gln
Dlg-KR15Q::GFP	pGU::GFP	Dlg::GFP with 15 Lys/Arg residues in PB mutated to Gln
Dlg-ΔPDZ::GFP	pGU::GFP	aa1-611 (PDZ domain) deleted from Dlg::GFP
Dlg-ΔPDZ-KR6Q::GFP	pGU::GFP	carrying KR6Q mutation in DlgΔPDZ::GFP
Dlg-ΔPDZ-KR15Q::GFP	pGU::GFP	carrying KR15Q mutation in DlgΔPDZ::GFP
GST-PB	pGEX-4T	Dlg-PB from Dlg::GFP (aa669-722) inserted into pGEX
GST-PB-KR6Q	pGEX-4T	Dlg-PB-KR6Q from DlgKR6Q::GFP (aa669-722) inserted into pGEX
GST-PB-KR15Q	pGEX-4T	Dlg-PB-KR15Q from DlgKR15Q::GFP (aa669-722) inserted into pGEX
Dlg-ΔGUK::GFP	pGU::GFP	aa768-983 (GUK domain) deleted from Dlg::GFP
Dlg-S4A::GFP	pGU::GFP	Phospho-serine residues 670, 684, 702, 713 mutated to Ala in Dlg::GFP
Dlg-ΔPDZ-S4A::GFP	pGU::GFP	aa1-611 (PDZ domain) deleted from Dlg-S4A::GFP
Dlg-S4A-ΔGUK::GFP	pGU::GFP	aa768-983 (GUK domain) deleted from Dlg-S4A::GFP
Dlg-m30::GFP	pGU::GFP	aa640 mutated from Leu to Pro in Dlg::GFP
Dlg-m30-ΔPDZ::GFP	pGU::GFP	aa1-611 (PDZ domain) deleted from Dlg-m30::GFP
Dlg-m30-ΔGUK::GFP	pGU::GFP	aa768-983 (GUK domain) deleted from Dlg-m30::GFP
Dlg^{R}::GFP	pGU::GFP	TAAGCTGCATGTG AAGCGAAA was converted to TAAACTCCACGTC AAACGCAAG from Dlg::GFP
Dlg-KR6Q^{R}::GFP	pGU::GFP	TAAGCTGCATGTG AAGCGAAA was converted to TAAACTCCACGTC AAACGCAAG from Dlg-KR6Q::GFP
Dlg-ΔGUK^{R}::GFP	pGU::GFP	TAAGCTGCATGTG AAGCGAAA was converted to TAAACTCCACGTC AAACGCAAG from DlgΔGUK::GFP
Dlg-S4A^{R}::GFP	pGU::GFP	TAAGCTGCATGTG AAGCGAAA was converted to TAAACTCCACGTC AAACGCAAG from DlgS4A::GFP
Dlg-m30^{R}::GFP	pGU::GFP	TAAGCTGCATGTG AAGCGAAA was converted to TAAACTCCACGTC AAACGCAAG from Dlgm30::GFP

SUPPLEMENTARY FIGURES:

Figure S1. Septate junctions in embryonic epithelial cells retain Dlg PM localization in redundancy to electrostatic PM targeting.

(**A**) PM Dlg::GFP in early (stage 7, "St 7") but not late (stage 14, "St 14") embryonic epithelia was sensitive to hypoxia. Stage 14 embryo also expressed Lgl::mCherry serving as a positive control for hypoxia treatment.

(**B**) PM Dlg::GFP in embryonic epithelial cells was sensitive to hypoxia in late stage embryos of *cora*$^{-/-}$ or *Atpα*$^{-/-}$. PM localization of Dlg$^{\Delta PDZ}$::GFP in late stage wild type embryo was also sensitive to hypoxia.

(**C**) PM localization of wild type and mutant Dlg::GFP in early and late embryonic epithelial cells. Embryos expressing Dlg$^{\Delta PDZ\text{-}KR6Q}$::GFP, Dlg$^{\Delta PDZ\text{-}KR15Q}$::GFP and Dlg$^{\Delta PDZ\text{-}S4A::GFP}$, were also expressing Lgl::mCherry (insets).

(**D**) Quantifications of PM localizations of wild type and mutant Dlg::GFP in **C**.

In parentheses: sample numbers.

Time stamps in A and B are in *hh:mm:ss* format. ****: $p<0.00001$; *: $p<0.001$; *ns*: $p>0.05$.

Figure S2. PM targeting of DlgΔGUK::GFP but not Dlg-S4A::GFP is sensitive to hypoxia.

(**A, B**) Selected frames of time-lapse recordings of *lgl::mCherry dlg*$^{\Delta GUK}$*::GFP* (A, Movie S5) or *lgl::mCherry dlg*^{S4A}*::GFP* (B, Movie S6) follicular cells undergoing hypoxia and reoxygenation.

(**A', B'**) Quantification of PM localizations of Lgl::mCherry and Dlg^{S4A}::GFP in A (A', n=24) and Lgl::mCherry and Dlg$^{\Delta GUK}$::GFP (B', n=15).

Time stamps in *hh:mm:ss* format.

Figure S3. Dlg^{R}::GFP and Dlg$^{\Delta PDZ}$::GFP are resistant to *dlg-RNAi*.

Dlg::GFP, but not Dlg^{R}::GFP or Dlg$^{\Delta PDZ}$::GFP, was efficiently knocked down in *dlg-RNAi* follicular cells (labeled by nuclear RFP).

SUPPLEMENTARY MOVIES

Movie S1. Acute and reversible loss of PM Dlg::GFP and Lgl::mCherry under hypoxia in follicular cells

Ovaries from a 2-day old *dlg::GFP lgl::mCherry* female were dissected and imaged live in an environment-controlled micro chamber. Hypoxic (0.5% O_2) gas was flashed into the chamber at 0 minute to induce hypoxia and normal air was flashed into chamber at 111 minutes for reoxygenation. Time intervals are 3 minutes during hypoxia and 10 seconds during reoxygenation. Note the incomplete loss of PM Dlg::GFP at the end of hypoxia. Time stamp: *hh:mm:ss*.

Movie S2. Acute and reversible loss of PM Dlg$^{\Delta PDZ}$::GFP and Lgl::mCherry under hypoxia

Ovaries from a 2-day old *lgl::mCherry*, *dlg$^{\Delta PDZ}$::GFP* female were dissected and imaged live similarly as in Movie S1. Reoxygenation started at 36 minutes in the movie. Time intervals are 1 minute during hypoxia and 10 seconds during reoxygenation. Time stamp: *hh:mm:ss*.

Movie S3. PM Dlg::GFP in *PI4KIIIα-RNAi* cells showed accelerated loss under hypoxia and delayed recovery under reoxygenation

dlg::GFP, PI4KIIIα-RNAi females were heat-shocked and ovaries were dissected three days after and imaged live similarly as in Movie S1. Reoxygenation starts at 96 minutes in the movie. Time intervals are 3 minutes during hypoxia and 10 seconds during reoxygenation. *PI4KIIIα-RNAi* cells were labelled by RFP. Time stamp: *hh:mm:ss*.

Movie S4. PM Dlg$^{\Delta PDZ}$::GFP in *PI4KIIIα-RNAi* cells showed accelerated loss under hypoxia and delayed recovery under reoxygenation

dlg$^{\Delta PDZ}$::GFP, PI4KIIIα-RNAi females were heat-shocked and ovaries were dissected three days after and imaged live similarly as in Movie S1. Reoxygenation starts at 20

minutes in the movie. Time intervals are 1 minute during hypoxia and 10 seconds during reoxygenation. *PI4KIIIα-RNAi* cells were labelled by RFP. Time stamp: *hh:mm:ss*.

Movie S5. PM localization of Dlg^{S4A}::GFP is resistant to hypoxia

Ovaries from a 2-day old *lgl::mCherry dlg^{S4A}::GFP* female were dissected and imaged live similarly as in Movie S1. Reoxygenation starts at 85 minutes in the movie. Time intervals are 1 minute during hypoxia and 10 seconds during reoxygenation. Time stamp: *hh:mm:ss*.

Movie S6. Acute and reversible loss of PM Dlg$^{\Delta GUK}$::GFP under hypoxia

Ovaries from a 2-day old *dlg$^{\Delta GUK}$::GFP; lgl::mCherry* female were dissected and imaged live similarly as in Movie S1. Reoxygenation starts at 92 minutes in the movie. Time intervals are 1 minute during hypoxia and 10 seconds during reoxygenation. Time stamp: *hh:mm:ss*.

Genotypes of *Drosophila* Samples in Figures.

Figure 1:

(C) *w; ubi-dlg::GFP/CyO*

w; ubi-dlg^{KR6Q}::GFP/CyO

w; ubi-dlg^{KR15Q}::GFP/CyO

w; ubi-dlg$^{\Delta PDZ}$::GFP/CyO

w; ubi-dlg$^{\Delta PDZ\text{-}KR6Q}$::GFP/CyO

w; ubi-dlg$^{\Delta PDZ\text{-}KR15Q}$::GFP/CyO

(D) *w dlg::GFP/+; lgl::mCherry/+*

w; ubi-dlg$^{\Delta PDZ}$::GFP/lgl::mCherry

Figure 2:

(A) *w UAS-mRFP-FKBP-5'Ptas/dlg::GFP;; hs-FLP Act5C(FRT.CD2)-Gal4 UAS-RFP^{NLS}/ UAS-Lck-FRB::CFP*

w UAS-mRFP-FKBP-5'Ptas/+; ubi-dlg$^{\Delta PDZ}$::GFP/+; hs-FLP Act5C(FRT.CD2)-Gal4 UAS-RFP^{NLS}/UAS-Lck-FRB::CFP

(B) *w dlg::GFP;; hs-FLP Act5C(FRT.CD2)-Gal4 UAS-RFP^{NLS}/UAS-PI4KIIIα-RNAi*

w; ubi-dlg$^{\Delta PDZ}$::GFP; hs-FLP Act5C(FRT.CD2)-Gal4 UAS-RFP^{NLS}/UAS-PI4KIIIα-RNAi

Figure 3:

(A) *w; ubi-dlg$^{\Delta GUK}$::GFP/CyO*

w; ubi-dlg^{S4A}::GFP/CyO

w; ubi-dlg$^{\Delta PDZ\text{-}S4A}$::GFP/CyO

w; ubi-dlg$^{S4A\text{-}\Delta GUK}$::GFP/CyO

w; ubi-dlg^{m30}::GFP/CyO

w; ubi-dlg$^{m30\text{-}\Delta PDZ}$::GFP/CyO

w;ubi-dlg$^{m30\text{-}\Delta GUK}$::GFP/CyO

(B) *w dlg::GFP;; hs-FLP Act5C(FRT.CD2)-Gal4 UAS-RFP^{NLS}/ UAS-scrib-RNAi*

w; ubi-dlg^{KR6Q}::GFP; hs-FLP Act5C(FRT.CD2)-Gal4 UAS-RFP^{NLS}/ UAS-scrib-RNAi

w; ubi-dlg$^{\Delta PDZ}$::GFP; hs-FLP Act5C(FRT.CD2)-Gal4 UAS-RFP^{NLS}/ UAS-scrib-RNAi

w; ubi-dlg^{S4A}::GFP; hs-FLP Act5C(FRT.CD2)-Gal4 UAS-RFP^{NLS}/ UAS-scrib-RNAi

w; ubi-dlg^{m30}::GFP; hs-FLP Act5C(FRT.CD2)-Gal4 UAS-RFP^{NLS}/ UAS-scrib-RNAi

w; ubi-dlg$^{\Delta GUK}$::GFP; hs-FLP Act5C(FRT.CD2)-Gal4 UAS-RFP^{NLS}/ UAS-scrib-RNAi

(C) *w dlg::GFP; ; hs-FLP Act5C(FRT.CD2)-Gal4 UAS-RFP^{NLS}/ UAS-lgl-RNAi*

w; ubi-dlg^{KR6Q}::GFP; hs-FLP Act5C(FRT.CD2)-Gal4 UAS-RFP^{NLS}/ UAS-lgl-RNAi

w; ubi-dlg$^{\Delta PDZ}$::GFP; hs-FLP Act5C(FRT.CD2)-Gal4 UAS-RFP^{NLS}/ UAS-lgl-RNAi

w; ubi-dlg^{S4A}::GFP; hs-FLP Act5C(FRT.CD2)-Gal4 UAS-RFP^{NLS}/ UAS-lgl-RNAi

w; ubi-dlg^{m30}::GFP; hs-FLP Act5C(FRT.CD2)-Gal4 UAS-RFP^{NLS}/ UAS-lgl-RNAi

w; ubi-dlg$^{\Delta GUK}$::GFP; hs-FLP Act5C(FRT.CD2)-Gal4 UAS-RFP^{NLS}/ UAS-lgl-RNAi

Figure 4:

(A) *w dlg$^{[A]}$ FRT^{19A}/ubi-RFP FRT^{19A}*

w dlg$^{[A]}$ FRT^{19A}/ubi-RFP FRT^{19A}; ubi-dlg::GFP/+

w dlg$^{[A]}$ FRT^{19A}/ubi-RFP FRT^{19A}; ubi-dlg$^{\Delta PDZ}$::GFP/+

w dlg$^{[A]}$ FRT^{19A}/ubi-RFP FRT^{19A}; ubi-dlg$^{\Delta GUK}$::GFP/+

w dlg$^{[A]}$ FRT^{19A}/ubi-RFP FRT^{19A}; ubi-dlg^{KR6Q}::GFP/+

w dlg$^{[A]}$ FRT^{19A}/ubi-RFP FRT^{19A}; ubi-dlg$^{\Delta PDZ\text{-}KR6Q}$::GFP/+

w dlg$^{[A]}$ FRT^{19A}/ubi-RFP FRT^{19A}; ubi-dlg^{S4A}::GFP/+

w dlg$^{[A]}$ FRT^{19A}/ubi-RFP FRT^{19A}; ubi-dlg^{m30}::GFP/+

w dlg$^{[A]}$ FRT^{19A}/ubi-RFP FRT^{19A} ubi-dlg$^{m30\text{-}\Delta PDZ}$::GFP/+

w dlg$^{[A]}$ FRT^{19A}/ubi-RFP FRT^{19A}; ubi-dlg $^{m30\text{-}\Delta GUK}$::GFP/+

(B) Top row:

w; ey-Gal4 UAS-Ras^{V12}/+

w; ey-Gal4 UAS-Ras^{v12}/+; UAS-dlg-RNAi/+

w; ey-Gal4 UAS-Ras^{V12}/ubi-dlg^{R}::GFP; UAS-dlg-RNAi/+

w; ey-Gal4 UAS-Ras^{V12}/ubi-dlg$^{\Delta PDZ}$::GFP; UAS-dlg-RNAi/+

w; ey-Gal4 UAS-Ras^{V12}/ubi-dlg$^{KR6Q\text{-}R}$::GFP; UAS-dlg-RNAi/+

Bottom row:

w; ey-Gal4/+; UAS-dlg-RNAi/+

w; ey-Gal4 UAS-Ras^{V12}/ubi-dlg$^{\Delta PDZ\text{-}KR6Q}$::GFP; UAS-dlg-RNAi/+

w; ey-Gal4 UAS-Ras^{V12}/ubi-dlg$^{m30\text{-}R}$::GFP; UAS-dlg-RNAi/+

w; ey-Gal4 UAS-Ras^{V12}/ubi-dlg$^{m30\text{-}KR6Q\text{-}R}$::GFP; UAS-dlg-RNAi/+

w; ey-Gal4 UAS-Ras^{V12}/ubi-dlg$^{m30\text{-}\Delta GUK\text{-}R}$::GFP; UAS-dlg-RNAi/+

Figure S1:

(A) *w*; *ubi-dlg::GFP/ubi-dlg::GFP*

w; ubi-dlg::GFP/Lgl::mCherry

(B) *w dlg::GFP/+; cora^{5}/ cora^{5}*

w dlg::GFP/+; Atpα^{DTS2A3}/ Atpα^{DTS2A3}

w; ubi-dlg$^{\Delta PDZ}$::GFP /CyO

(C) Top row:

w; ubi-dlg::GFP/CyO

w; ubi-dlg^{KR6Q}::GFP /CyO

w;ubi-dlg^{KR15Q}::GFP /CyO

w; ubi-dlg^{S4A}::GFP /CyO

w; ubi-dlg^{m30}::GFP /CyO

Bottom row:

w; ubi-dlg$^{\Delta PDZ}$::GFP/CyO

w; ubi-dlg$^{\Delta PDZ\text{-}KR6Q}$::GFP / lgl::mCherry

w; ubi-dlg$^{\Delta PDZ\text{-}KR15Q}$::GFP / lgl::mCherry

w; ubi-dlg$^{\Delta PDZ\text{-}S4A}$::GFP / lgl::mCherry

Figure S2:

(A) *w; ubi-dlg$^{\Delta GUK}$::GFP / lgl::mCherry*

(B) *w; ubi-dlg^{S4A}::GFP / lgl::mCherry*

Figure S3:

(A) *w dlg::GFP/+; UAS-dlg-RNAi/+; hs-FLP Act5C(FRT.CD2)-Gal4 UAS-RFP^{NLS} /+*

(B) *w; UAS-dlg-RNAi /ubi-dlg^{R}-GFP; hs-FLP Act5C(FRT.CD2)-Gal4 UAS-RFP^{NLS} /+*

(C) *w; dlg-RNAi /ubi-dlg$^{\Delta PDZ}$-GFP; hs-FLP Act5C(FRT.CD2)-Gal4 UAS-RFP^{NLS} /+*

Figure S1

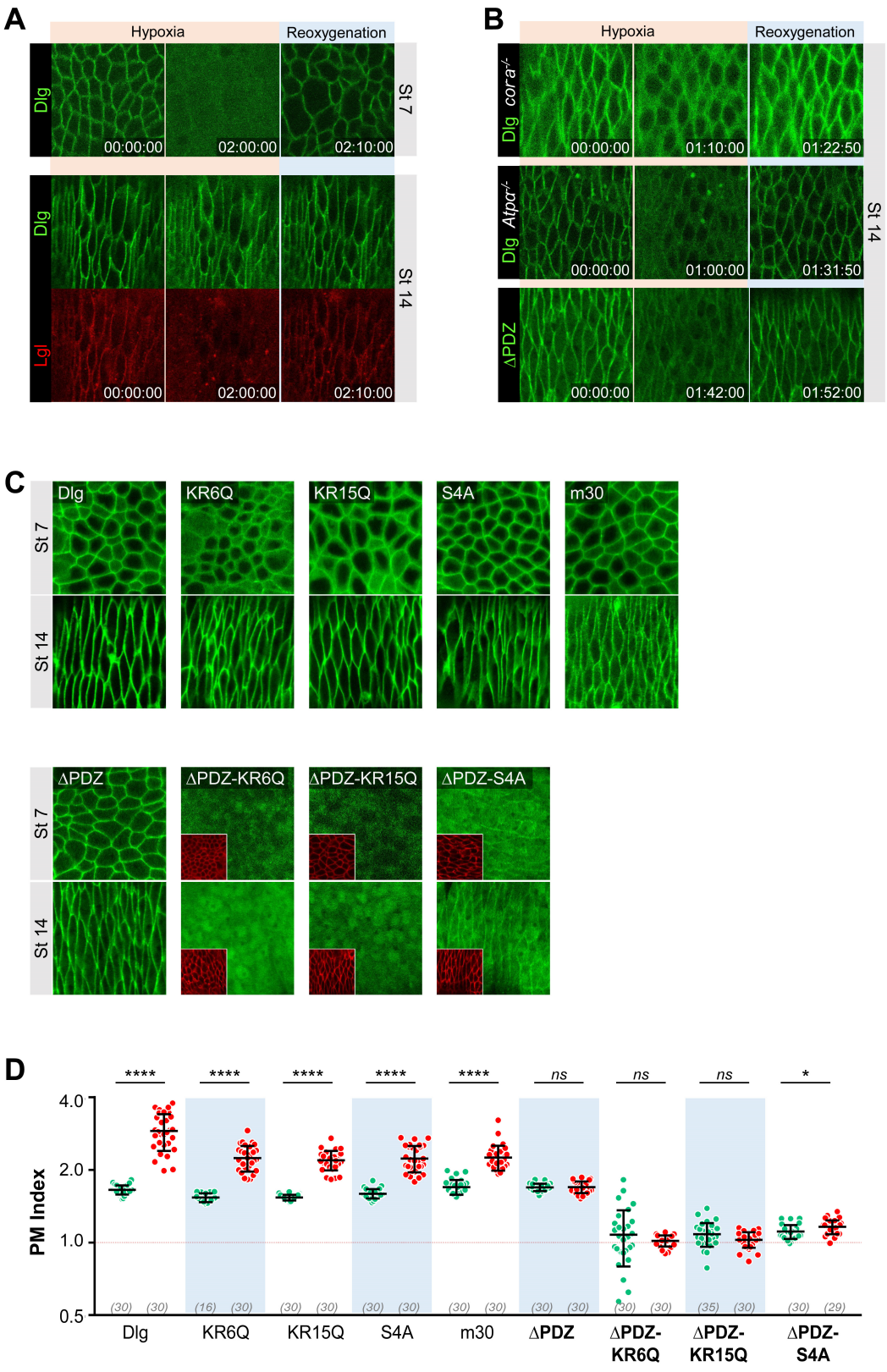

Figure S2

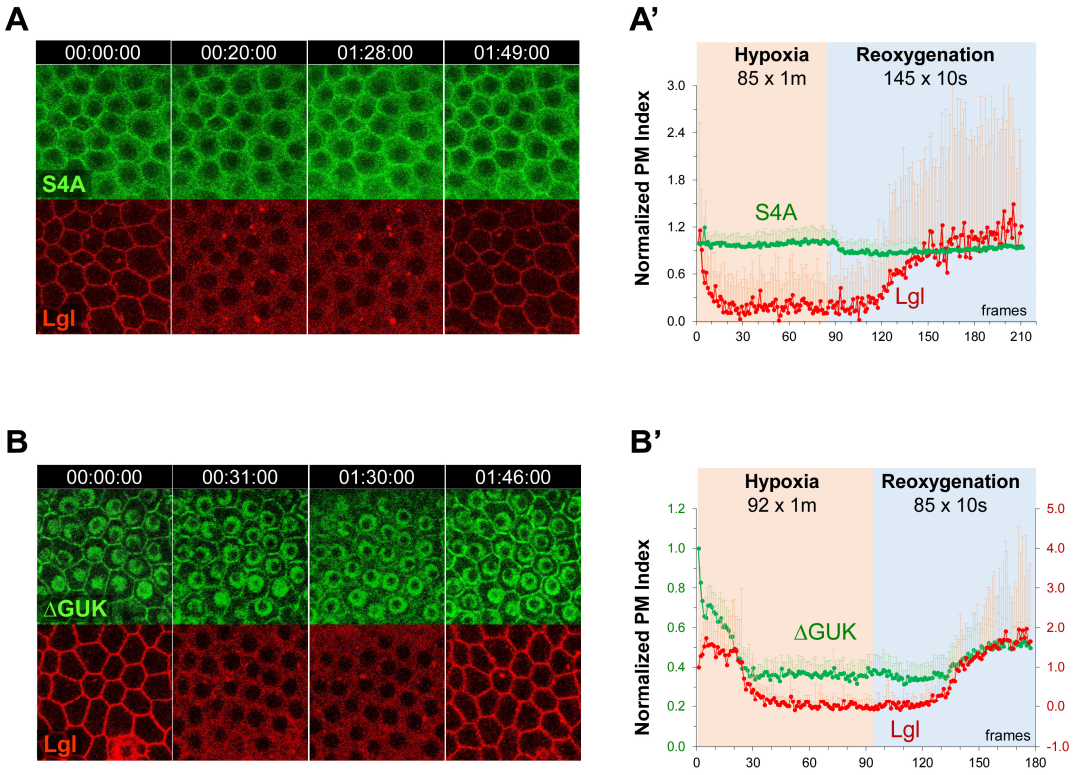

Figure S3